

Research Paper

Phase and Size Controllable Synthesis of NaYbF₄ Nanocrystals in Oleic Acid/ Ionic Liquid Two-Phase System for Targeted Fluorescent Imaging of Gastric Cancer

Liyuan Pan¹, Meng He¹, Jiebing Ma¹, Wei Tang², Guo Gao¹, Rong He¹✉, Haichuan Su³✉, Daxiang Cui¹✉

1. Department of Bio-Nano Science and Engineering, Key Laboratory for Thin Film and Microfabrication of Ministry of Education, Institute of Micro-Nano Science and Technology, Shanghai Jiao Tong University, 800 Dongchuan Road, Shanghai 200240, P. R. China;
2. Key laboratory for Ultrafine Materials of ministry of Education, Engineering Research Center for Biomedical material of Ministry of Education, East China University of Science and Technology, Shanghai, 200237, P. R. China;
3. Department of Oncology, Tangdu Hospital, Fourth Military Medical University, 8Xinsi Road, Xi'an 71008, P. R. China.

✉ Corresponding author: Shanghai Jiao Tong University, 800 Dongchuan Road, Shanghai 200240, P. R. China. dxcui@sjtu.edu.cn (D.X. Cui). E-mail: rhe@sjtu.edu.cn (R. He). Or shc@fmmu.edu.cn (H. C. Su). Tel: (+86) 21 34206886 Fax: (+86) 21 34206886

© Ivyspring International Publisher. This is an open-access article distributed under the terms of the Creative Commons License (<http://creativecommons.org/licenses/by-nc-nd/3.0/>). Reproduction is permitted for personal, noncommercial use, provided that the article is in whole, unmodified, and properly cited.

Received: 2012.09.27; Accepted: 2012.11.21; Published: 2013.02.27

Abstract

Upconversion nanocrystals with small size and strong fluorescent signals own great potential in applications such as biomolecule-labeling, *in vivo* tracking and molecular imaging. Herein we reported that NaYbF₄: 25%Gd, 2%Tm upconversion nanocrystals with small size and strong fluorescent signals were controllably synthesized by oleic acid (OA)/ ionic liquid (IL) two-phase system for targeted fluorescent imaging of gastric cancer *in vivo*. The optimal synthesis condition of NaYbF₄: 25%Gd, 2%Tm upconversion nanocrystals by OA/IL two-phase system was established, adding more metal ion such as Na⁺ ion could facilitate the size control and crystal-phase transition, more importantly, markedly enhancing fluorescent intensity of beta-phase nanocrystals compared with traditional methods. Alpha-phase NaYbF₄: 2%Tm upconversion nanocrystals with less than 10nm in diameter and beta-phase NaYbF₄: 25%Gd, 2%Tm upconversion nanocrystals with 30 nm or so in diameter and strong fluorescent signals were obtained, these synthesized nanocrystals exhibited very low cytotoxicity. Folic acid-conjugated silica-modified beta-phase NaYbF₄: 25%Gd, 2%Tm upconversion nanocrystals were prepared, could actively target gastric cancer tissues implanted into nude mice *in vivo*, and realized targeted fluorescent imaging. Folic acid-conjugated silica-modified NaYbF₄: 25%Gd, 2%Tm upconversion nanocrystals show great potential in applications such as targeted near infrared radiation fluorescent imaging, magnetic resonance imaging and targeted therapy of gastric cancer in the near future.

Key words: NaYbF₄: 25%Gd, 2%Tm upconversion nanocrystals, synthesis, targeted imaging, fluorescent imaging, gastric cancer, cytotoxicity.

Introduction

In recent years, lanthanide (Ln)-doped upconversion nanocrystals (UCNPs) have attracted broad attention because of their unique optical properties

such as narrow bandwidth, long-lived emission, large anti-Stokes shifts and ligand-dependent luminescence sensitization [1-5]. Due to their good biocompatibility

and near infrared radiation (NIR) imaging, lanthanide (Ln) doped UCNPs exhibit great potential in applications such as biomolecule-labeling, *in vivo* tracking, and molecular imaging [6-10]. Upconversion luminescent nanocrystals exhibit distinctive advantages over conventional luminescent materials such as quantum dots (QDs) and organic fluorescent dyes. Both QDs and organic dyes are generally excited with ultraviolet (UV) and visible light, which may cause photo-damage and gene mutation of biological samples. Organic dyes often suffer from intrinsic photobleaching and low emission efficiency [11-16]. QDs exhibit high quantum yield, high photostability and size-dependent tunable emission, being attractive alternative luminescent labels for ultrasensitive detection and molecular imaging. However, there are several factors to limit the use of QDs for bio-imaging. For example, QDs may threaten human health due to the fact that typical QDs are composed of heavy metals (e.g., CdSe) and can easily penetrate into cells [11, 12]. Intermittent emission (blinking) of QDs also leads to a limited use for bio-imaging. Conversely, UCNPs have many merits such as the absence of photo-damage to live organisms, low autofluorescence background, high signal-to-noise ratio and high detection sensitivity, and high light penetration depth in biological tissues, exhibiting great potential in applications such as *in vitro* and *in vivo* optical imaging [17]. In addition, UCNPs were excited by NIR light, which has the deep penetration ability and is very safe to human body and cells [18, 19].

In recent years, great efforts have been made to the controllable synthesis of rare earth (RE) fluoride nanocrystals. In particular, high quality fluoride nanocrystals have been synthesized successfully through chemical methods such as hydro (solvo) thermal reaction, thermal decomposition of RE organic precursors and the emerging ionic liquids (ILs) method [20]. However, the three reaction systems still have some significant drawbacks. For example, in the typical hydro (solvo) thermal reaction system, it is still very difficult to control the crystal phase and maintain small size (<50 nm) simultaneously [21-23]. The thermal decomposition system needs rigorous experimental conditions such as high temperature (>300°C), inert gas protection, waterless environment, and toxic organic precursors. In order to solve these problems, our group established the oleic acid (OA)/ionic liquid (ILs) two-phase system, combining the features of thermal decomposition (size and morphology control) and IL-based strategy (mild conditions, environment-friendly reagents and direct water-solubility) [24], which has been successfully used to prepare highly uniform and monodisperse

rare earth fluoride nanocrystals with less than 50 nm in diameter. For example, water-soluble hexagonal NaREF₄ nanocrystals were obtained by adding n-octanol [25], high-quality lanthanide-doped NaGdF₄ upconversion nanocrystals with different crystal-phases also were obtained in OA-phase and IL-phase through a one-step controllable reaction, and the synthesized lanthanide-doped NaGdF₄ upconversion nanocrystals also were successfully used for dual-modality UCL imaging and CT imaging [26], water-soluble hexagonal rare earth (RE= La, Gd and Y) fluoride nanocrystals with uniform morphology were also obtained, IL (BmimPF₆) and n-octanol played key roles in transforming phase structure and controlling particle size [27]. Upconversion nanocrystals such as NaREF₄ exhibited two polymorphic forms, namely cubic (α) and hexagonal (β) phases, of which β -NaYF₄: Yb, Er/Tm nanocrystals displayed excellent performance in biomolecule-labeling and molecular imaging. It is confirmed that the maximal NIR-to-NIR UCPL output of NaYbF₄: 2%Tm nanocrystals was three to four times higher than that of NaYF₄: 20%Yb, 2%Tm [28, 29]. However, up to date, no report is associated with the synthesis of NaYbF₄: 25%Gd, 2%Tm upconversion nanocrystals via OA/ILs two-phase system.

It is well known that gastric cancer is currently the fourth most common cancer in the world, and the second most common cancer and second most common cause of cancer-related death in China [30-32]. Gastric cancer remains difficult to cure because most patients were present with advanced disease [33]. Therefore, how to recognize and track early gastric cancer cells is one key problem for diagnosis and therapy of early gastric cancer. Since 1998, we have been trying to establish an early gastric cancer pre-warning system [34, 35]. In order to find *in vivo* early gastric cancer cells, we selected potential biomarkers associated with gastric cancer, combined nanoparticles and molecular imaging techniques, and tried to identify early gastric cancer cells *in vivo* [36-44]. However, up to date, there are no real safe efficient multi-functional nanoprobe that have been successfully developed to recognize early gastric cancer cells *in vivo*. Therefore, how to develop safe, efficient nanoprobe to recognize early gastric cancer cells *in vivo* has become our major concerns.

Herein we used novel OA/IL two-phase system to prepare a uniform size and phase NaYbF₄: 25% Gd, 2%Tm upconversion nanocrystals, and investigated the influence of Na⁺ concentration and the introduction of RE³⁺ on the size control and phase transition, and then optimized the synthesis condition, prepared folic acid-conjugated β -phase core/shell NaYbF₄:

25%Gd, 2%Tm@SiO₂ nanoprobe. prepared nanoprobe were injected into the nude mice models loaded with gastric cancer cells, and investigated the feasibility of their use as contrast reagents for targeted NIR fluorescent imaging of gastric cancer tissues *in vivo*. Results showed that highly uniform and monodisperse cubic NaYbF₄, 2%Tm (α -phase) and hexagonal NaYbF₄: 25%Gd, 2%Tm (β -phase) nanocrystals with small size and strong fluorescent signals were obtained in the OA/IL two-phase system. The ideal luminescence nanocrystals were successfully used for targeted fluorescent imaging of gastric cancer tissues *in vivo*. The folic acid-conjugated NaYbF₄:25%Gd, 2%Tm@SiO₂ nanocrystals show great potential in applications such as targeted NIR imaging, MRI and treatment of early gastric cancer in the near future.

Materials and Methods

Synthesis of hydrophobic cubic-phase NaYbF₄, 2%Tm nanocrystals

RE(oleate)₃ complexes were prepared by previously reported methods [45, 46]. OA-capped UCNP were synthesized by a novel OA/IL two-phase system [27]. 1mmol of RE(oleate)₃ [Yb: Tm] = [98: 2] and a stoichiometric amount of sodium oleate were mixed together in a 50-mL Teflon-lined autoclave which contained 15 mL of BmimBF₄ and 10mL of oleic acid. The two-phase system was sealed and maintained at 240 °C for 24 h. The precipitates can be found on the interface of the two phase system when the products were cooled to room temperature naturally. Then, they were washed by cyclohexane and ethanol several times to remove the extra oleic acid and other remnants under ultrasonic conditions, and were collected through centrifugation at 8500 rpm. Finally, the products were dried at 65 °C under vacuum for 12 h.

Synthesis of hydrophilic hexagonal-phase NaYbF₄: 25%Gd, 2%Tm nanocrystals in IL-phase

1mmol of RE(oleate)₃ [Yb: Gd: Tm] = [73: 25: 2] and the amount of 130 mol% sodium oleate were mixed together in a 50-mL Teflon-lined autoclave in order to prepare a uniform hexagonal-phase nanocrystals. The synthetic procedure was nearly the same as that used to synthesize the cubic-phase products except that 30 mL of BmimBF₆ ionic liquid was added to the two-phase system instead of 15 mL of BmimBF₄. The products were separated through centrifugation at 9500 rpm and then they were collected by purifying the precipitates with cyclohexane and ethanol several times to remove oleic acid, ionic liquid, and other remnants. The products were dried at 65 °C under

vacuum overnight.

Silica coating on hexagonal-phase NaYbF₄: 25%Gd, 2% Tm nanocrystals

In a 25ml vial, 0.1 mmol of as-prepared NaYbF₄: 25%Gd, 2%Tm UCNP were dispersed in 5 mL of ethanol, then 0.1 mL of ammonium hydroxide (28%wt in water) was dropped. Thereafter 15mL ethanol containing 120 μ L TEOS was added quickly with vigorous stirring. The solution was stirred at room temperature for 24 h. Finally, the silica-coated products were collected by adding deionized water and centrifuging to precipitate the products at a speed of 8500 rpm. The products were further purified by washing with ethanol and water several times to remove the residual reagents.

Synthesis of the amine-functionalized nanocrystals (UCNP@SiO₂-NH₂)

In a 100 mL glass flask, 1mmol of as-prepared silica-coated NaYbF₄: 25%Gd, 2%Tm UCNP were dispersed in 30mL of ethanol by sonication. Next, 10mL APS was added to the solution and the mixture is stirred and refluxed at 83°C for 4h. Then, they were repeatedly washed with ethanol and water several times.

Synthesis of the folic acidconjugated nanocrystals (UCNP -FA)

The folic acid conjugated UCNP nanocrystals were prepared by conjugating the amine-functionalized UCNP@SiO₂-NH₂ (NaYbF₄: 25 mol% Gd, 2 mol% Tm) with activated folic acid(FA). In brief, FA (120 mg, 2.72 \times 10⁻⁴mol) was dissolved in 25mL anhydrous dimethylsulfoxide (DMSO). EDC and NHS (molar ratio of FA/EDC/NHS=1:1:2.5) were added, and the mixture was stirred gently at room temperature for 1 h. UCNP@SiO₂-NH₂ nanocrystals (30mg) dissolved in DMSO (20 mL) were added to the activated FA solution, and the mixture was stirred gently for 3h at room temperature. The resultant precipitates were separated by centrifugation at 12000 rpm for 15 min and subsequently washed 3 times with PBS (pH 7.4). The powder was then dried under vacuum.

Cytotoxicity of UCNP@SiO₂-NH₂ nanocrystals before and after FA conjugation

In vitro cytotoxicity of prepared UCNP to human gastric cancer cell line MGC-803 cells was measured by using CCK-8 kit. The human gastric cancer cell line MGC803 cells were cultivated in Roswell Park Memorial Institute medium (RPMI) 1640 (Gibco, Invitrogen Corp., Carlsbad, CA) medium supple-

mented with 10% fetal bovine serum (FBS) and 1% penicillin in 96-well plate 5% CO₂, 37 °C for 24 h. The density of cells in a 96-well plates is 4×10³ cells /well (the 36 peripheral wells were filled with PBS, the remaining was control group). On the second day, different volume of UCNP@SiO₂-NH₂ nanocrystals before and after FA conjugation were dissolved in culture medium and the final concentration was 50, 100, 200, 400, 800 µg/mL. Thereafter, the medium was removed and cells were washed with PBS for two times. Cell viability was evaluated by CCK-8 kit, the optical absorbance of the solution was measured at 450 nm with 96-well microplate reader (Perkin Elmer). Results are calculated as percentages relative to control cells. Data are mean ±SD from three independent experiments.

Confocal luminescence imaging of cells incubated with UCNPs

Confocal luminescence imaging of cells was performed with a modified Leica laser-scanning microscope, with a CW NIR laser at λ =980 nm as the excitation source. UCNPs were excited by the external laser at 980 nm. And the emissions were collected in the ranges of λ= 400–800 nm for UCNPs. Cells were respectively cultured on 20mm glass cover slips in 6-well plates (2.5×10⁵cells/well) and pre-incubated for 24h. Then, MGC803 and GES cells were cultured in 2mL PBS contain UCNP-FA nanocrystals (200 µg/mL) instead of medium for 1 h at 37 °C. Another group MGC803 cells were incubated with UCNP@SiO₂-NH₂, and the third group MGC803 cells were incubated with excess free FA and UCNP-FA nanocomposites under the same conditions for competition experiments. All cells were washed three times with PBS solution and cells were fixed with 4% paraformaldehyde solution for 15 minutes at room temperature. Afterwards, PBS was used to rinse cells twice and the glass cover slips were transferred onto glass slides with 30% glycerol mounting medium.

Nude mice models with gastric cancer and in vivo imaging

All animal experiments (No.SYXK2007-0025) were approved by the Institutional Animal Care and Use Committee of Shanghai Jiao Tong university. Nude mice were obtained from Shanghai SLAC Laboratory Animal Co. Ltd (Shanghai, China). Animal procedures were in agreement with the guidelines of the Institutional Animal Care and Use Committee. Eight nude mice (4weeks old, 17±2g) were randomly divided into two groups such as intravenous injection group and control group, four mice per group. UCNP-FA or UCNP@SiO₂-NH₂ aqueous solution

(250µL 400µg/ mL) in PBS was injected into the nude mice via the tail vein after the mice were anesthetized with 100 µL 10% chloral hydrate for half an h. The images of mice at 4 h post-injection were recorded by a modified IVIS Lumina XR (Xenogen Corporation-Caliper, Alameda, CA,USA) with an external 0 ~ 5 W adjustable CW infrared laser (980 nm, Shanghai Connet Fiber Optics Co., China) as the excited source.

Statistical Analysis

All data were presented in this paper as means value ± S.D. Statistical differences were evaluated using the *t*-test and considered significance at *P* < 0.05 level.

Results and Discussions

Synthesis and characterization of cubic-phase UCNPs

The α-phase NaYbF₄, 2%Tm nanocrystals were synthesized by an OA/IL two-phase synthesis system. As shown in Figure 1, all the α-phase UCNPs exhibited spherical in shape, high uniformity and monodispersity. The average diameter of these nanoparticles was 7.76 ± 1.19 nm, which was confirmed by a detailed analysis of around 190 nanoparticles. Supplementary Material: Figure S1a shows the size distribution of oil-dispersible α-phase NaYbF₄, 2%Tm nanocrystals. The size distribution is consistent with a Gaussian distribution. In addition, HR-TEM image (Fig. 1C) shows the lattice distance of 0.30 nm, corresponding to *d* spacing for the (111) lattice plane of the α-phase NaYbF₄ structure. X-Ray diffraction (XRD) analysis was conducted to determine the phase structure of NaYbF₄, 2%Tm in the OA phase (Supplementary Material: Fig. S2). The XRD pattern for NaYbF₄, 2%Tm agrees well with the cubic-phase NaYbF₄ (JCPDS: 77-2043). Figure 1D shows clear diffraction rings corresponding to the specific (111),(200),(220), (311),(331) and (400) planes of α-phase NaYbF₄ lattice.

Synthesis and characterization of hexagonal phase UCNPs

As shown in Figure 3A, the β-phase NaYbF₄: 25%Gd, 2%Tm UCNPs were a mixture of round-shaped nanocrystals and elongated nanocrystals with the diameter of 32.13 ± 7.76 nm. The particle size distribution is given in Supplementary Material: Figure S1b. We can clearly see products in IL phase are much bigger than that synthesized in OA phase. In addition, HR-TEM image (Fig. 3C) shows the lattice distance of 0.51 nm, corresponding to *d* spacing for the (100) lattice plane of the hexagonal NaYbF₄ struc-

ture. The crystal phase of the products was further characterized by X-ray diffraction (XRD) data, as shown in Figure 2f. Figure 4D shows diffraction rings corresponding to the specific (100), (110), (111), (200), (201) (210), and (211) planes of hexagonal NaYbF₄ lattice. The upconversion luminescence (UCL) spectrum of Tm³⁺ doped β-phase UCNPs nanocrystals is shown in Supplementary Material: Figure S3, which showed that the fluorescent intensity of prepared beta-phase UCNPs was markedly enhanced comparing to conventional β-phase NaYbF₄ UCNPs.

According to the spectra of Tm³⁺ doped products, under excitation of CW laser at 980 nm, four distinct Tm³⁺ emission bands at 450, 475, 695 and 800 nm were identified. They originated from ¹D₂/³F₄, ¹G₄/³H₆, ³F₃/³H₆ and ³H₄/³H₆ transitions of Tm³⁺, respectively. Obviously the predominant NIR emission band at around 800 nm is assigned to the ³H₄/³H₆ transition, indicating that radiative deactivation of the upconverted energy predominantly occurs through NIR luminescence, which is favorable for bioimaging.

In fact, water-soluble NaYbF₄ nanocrystals with a pure hexagonal phase (β-phase) were not easily obtained. As disclosed in Figure 2a, the NaYbF₄, 2%Tm nanocrystals are a mixture of α-phase and β-phase nanocrystals. Pure β-NaYbF₄ was not achieved even when we added 30mL BmimPF₆ to the mixture and kept the system heated at 240 °C for 24 h [38]. Therefore, in this study, Gd³⁺ ions were introduced at different doping levels to trigger phase transformation in upconversion NaYbF₄, 2%Tm nanocrystals. The pure hexagonal phase of NaYbF₄, 2%Tm was obtained when 50 mol% Gd³⁺ ions were added in the first place (Fig. 2b). Then, we try to reduce the amount of Gd³⁺ ions. But when the amount of Gd³⁺ ions was set at 30mol % and 25mol%, we found α-phase and β-phase of NaYbF₄,Tm exist simultaneously and the XRD pattern were shown in Figure 2d and Figure 2e. After a serial of experiments, it is found that increasing the volume of sodium oleate might lead to the α→β phase transition, so the ratio of Na⁺ : RE³⁺ was increased to 1.3:1 and it turned out the pure hexagonal phase of NaYbF₄, 2%Tm can be obtained (Fig. 2c and Fig. 2f).

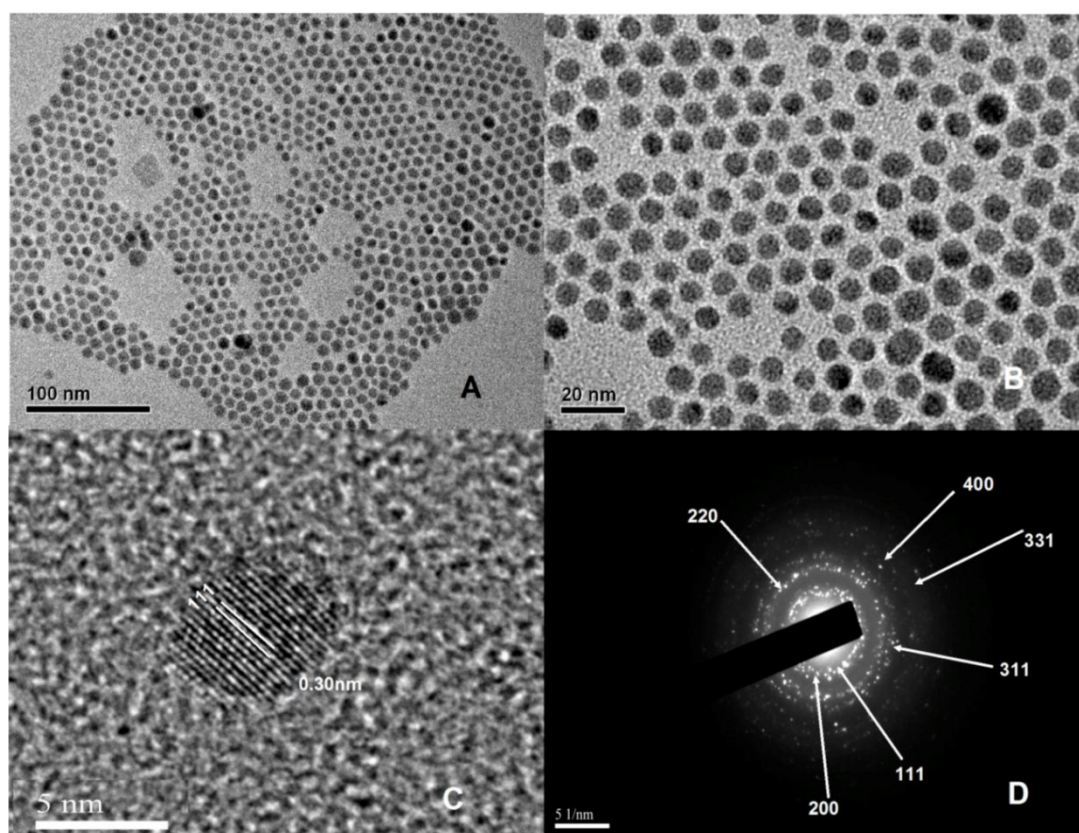


Figure 1. (A) and (B) TEM images with different magnifications of hydrophobic NaYbF₄, 2%Tm nanocrystals. (C) The corresponding HR-TEM image. (D) The SAED pattern.

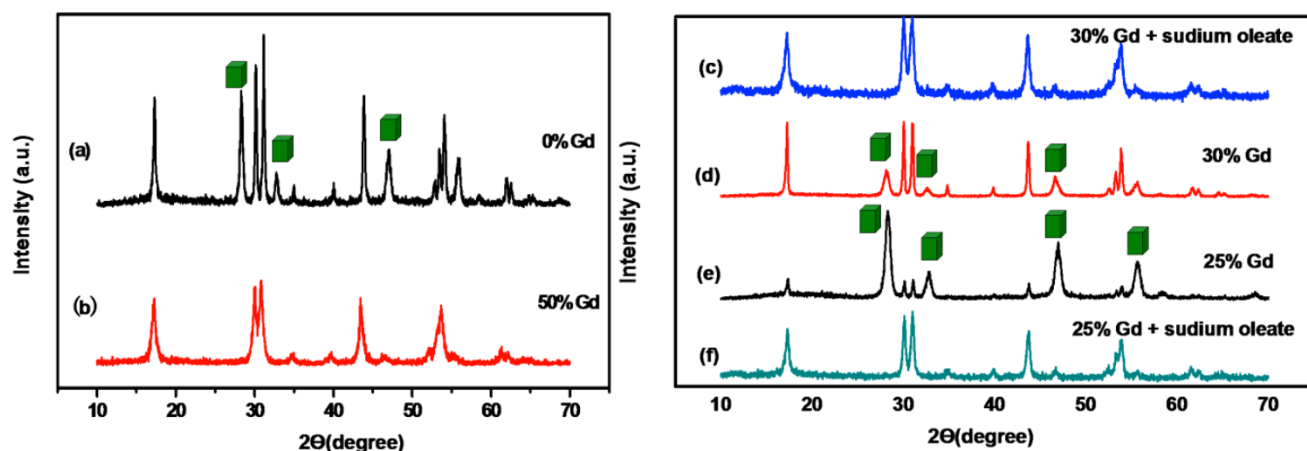


Figure 2. XRD patterns of NaYbF₄, 2%Tm nanocrystals fabricated under different conditions: (a) 30 mL BmFimPF₆. (b) 30 mL BmimPF₆ and 50 mol% Gd(oleate)₃. (c) 30 mL BmimPF₆, 30 mol% Gd(oleate)₃ and excess sodium oleate. (d) 30 mL BmFimPF₆ and 30 mol% Gd(oleate)₃. (e) 30 mL BmimPF₆, 25 mol% Gd(oleate)₃. (f) 30 mL BmimPF₆, 25 mol% Gd(oleate)₃ and excess sodium oleate. The peaks marked with a cubic box refer to cubic-phase NaYbF₄.

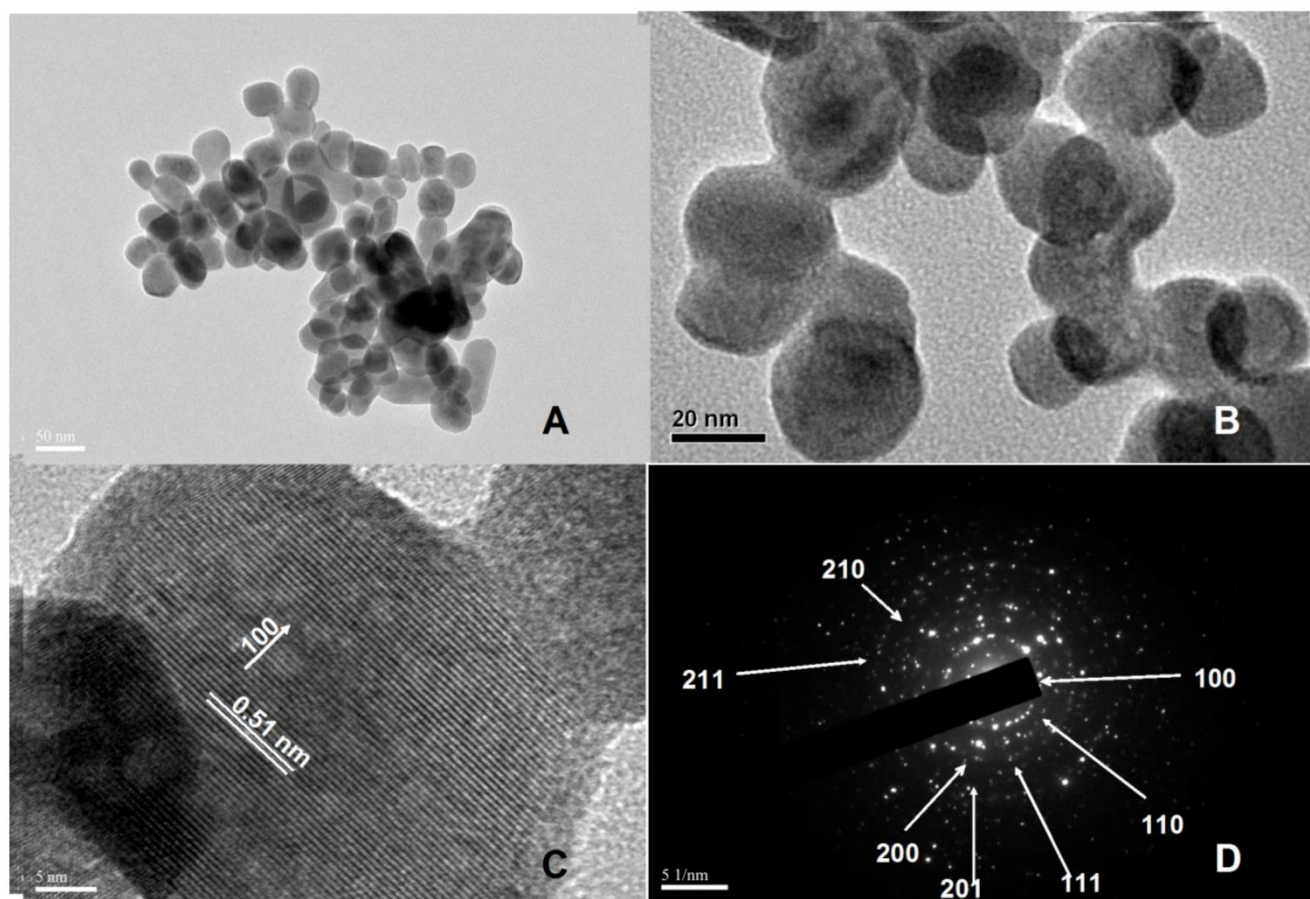


Figure 3. (A) and (B) TEM images with different magnifications of water-soluble hexagonal phase NaYbF₄: 25%Gd, 2%Tm nanocrystals. (C) The corresponding HR-TEM image. (D) The SAED pattern.

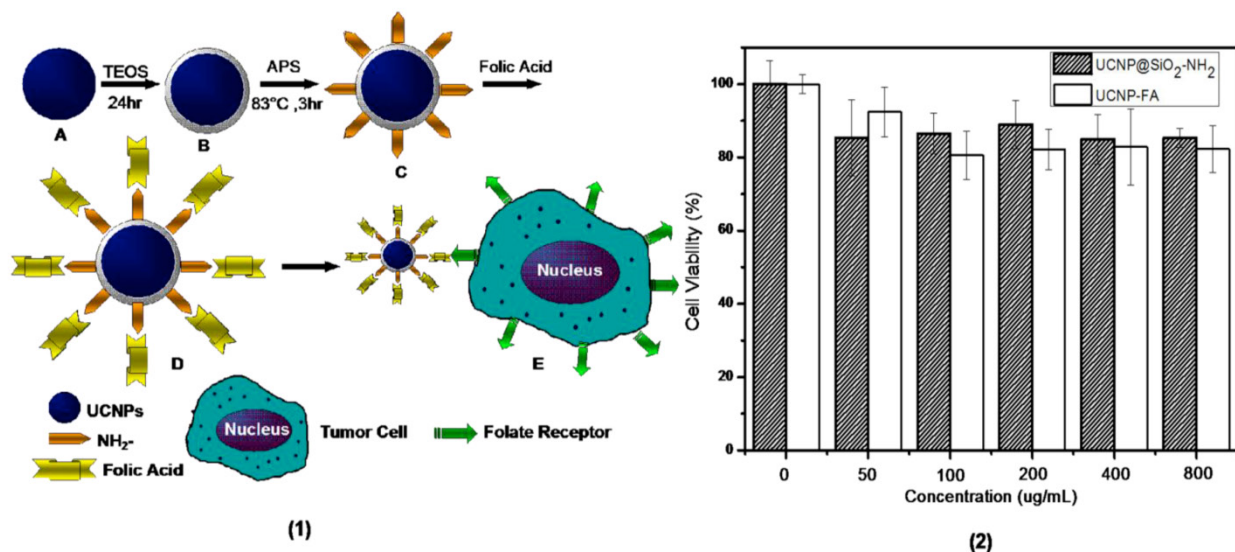


Figure 4. (1) Schematic diagram showing the synthesis of UCNP-FA (short for UCNP@SiO₂-NH-FA) core-shell nanocrystals: (A) water-soluble hexagonal phase NaYbF₄: 25%Gd, 2%Tm nanocrystals. (B) NaYbF₄: 25%Gd, 2%Tm@SiO₂ nanocrystals. (C) amine-functionalized UCNP@SiO₂-NH₂ core-shell nanocrystals. (D) UCNP-FA nanocrystals. (E) folate-mediated targeting with FR-positive tumor cells. (2) In vitro cell viability of MGC-803 cells incubated with UCNP@SiO₂-NH₂ and UCNP-FA nanocrystals at different concentrations for 24 h.

With regard to its $\alpha \rightarrow \beta$ phase transition behavior, NaREF₄ along the rare-earth series can be divided into three groups (I: Pr and Nd; II: Sm to Tb; III: Dy to Lu, Y) [47]. The corresponding RE fluorides of different group has different growing behavior and crystal structures with the radii changing. So we find the pure hexagonal phases of some RE fluorides are easily obtained in the OA/IL synthesis system, the others are not easily obtained. For example, the pure hexagonal NaGdF₄ and NaYF₄ are much easier to be obtained in the OA/IL system comparing to NaYbF₄. Nanocrystals can be tuned in phase (cubic or hexagonal) through the use of trivalent lanthanide dopant ions introduced at precisely defined concentrations [23]. For the OA/IL synthesis system, β -NaREF₄ in groups I and II was synthesized easily (such as La and Gd), while those in group III are not easily synthesized. In the structure of cubic sodium rare earth (RE) fluoride systems (NaREF₄), Na and RE cations are randomly distributed in the cationic sub-lattice. In contrast, in the hexagonal sodium rare earth (RE) fluoride systems, the cation sites have three types: a one-fold site occupied by RE³⁺, a one-fold site occupied randomly by 1/2Na⁺ and 1/2RE³⁺, and a two-fold site occupied randomly by Na⁺ and vacancies [48]. According to previous reports [49], compared with the Ln elements with larger ionic radius

(such as Gd³⁺), those with smaller ionic radius (such as Yb³⁺) have higher energy barriers for the synthesis of hexagonal products. Importantly, light lanthanides with large ionic radii show a high tendency towards electron cloud distortion due to increased dipole polarizability, and thus favor the hexagonal structures. We adopted the method of doping the lanthanide ions (such as Gd³⁺) with a size larger than Yb³⁺ in NaYbF₄ host lattices, this should dominate the formation of pure hexagonal-phase NaYbF₄ nanocrystals [23].

The formation process of NaREF₄ is that the C₁₇H₃₃COO⁻ bonded with RE³⁺ is gradually replaced by PF₆⁻, then when the whole system reaches a certain temperature, F⁻ anions are released from the cleavage of P-F bond to react with RE³⁺ ions. As we known, C₁₇H₃₃COO⁻ has a strong coordination capacity with RE³⁺ ions, we believe the increasing volume of sodium oleate will make the competition between PF₆⁻ anions and C₁₇H₃₃COO⁻ much fiercer which slows down the formation process of NaREF₄ and facilitate the anisotropic growth and lead to the formation of hexagonal structure. It is also possible because the increasing volume of Na³⁺ ions makes it easier to occupy the sites in the cationic sublattice. Scheme 1 (Figure A) shows the process of the formation of hexagonal RE fluoride nanocrystals in an OA/IL two-phase synthesis system.

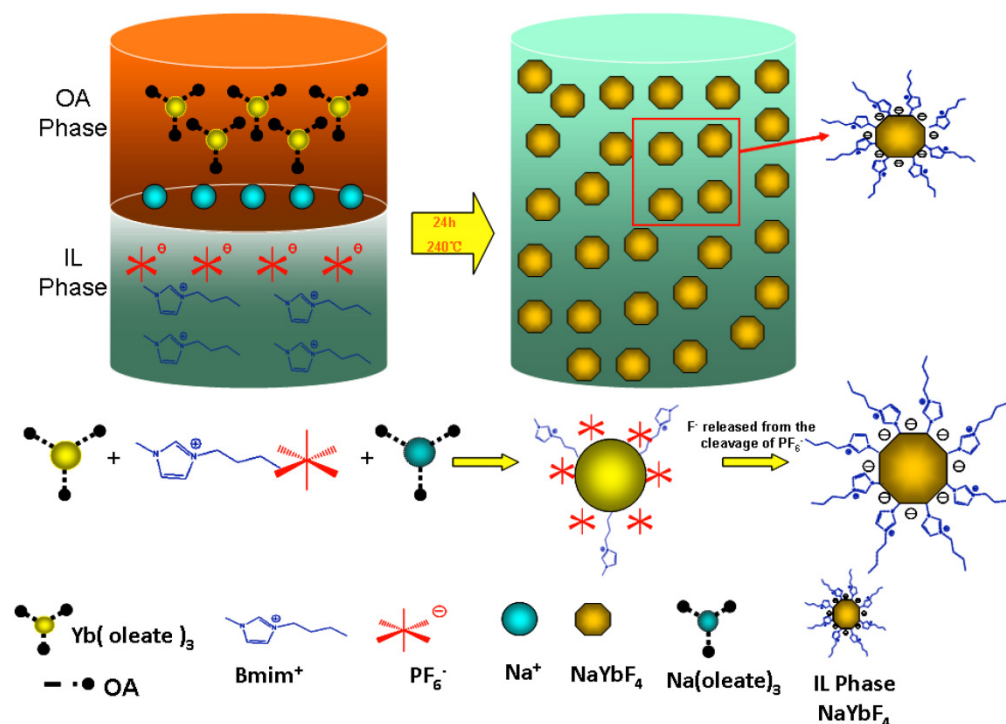


Figure A. (Scheme 1) Schematic diagram showing the mechanism for formation IL-capped RE fluoride nanocrystals in an OA/IL two-phase system.

Synthesis and characterization of UCNP-FA core-shell nanocrystals

To enhance stability and explore the biological application of the as-prepared products, silica coating was conducted to improve the biocompatibility of UCNPs while maintaining strong luminescent intensities. The Stöber method, which is performed in polar solvent and suitable for hydrophilic products, was used to coat silica onto the IL-capped hexagonal UCNPs. Also the IL ligands on the surface of the as-prepared products make them disperse in water or ethanol and allow their affinity to silica easily. As disclosed in Supplementary Material: Figure S4b, a thin layer silica shell with a thickness of approximately 8.17 nm surrounded the surface of $\text{NaYbF}_4:25\%\text{Gd}$, 2%Tm nanocrystals. FT-IR and energy-dispersive X-ray (EDX) analysis revealed the successful silica coating on the surface of $\text{NaYbF}_4:25\%\text{Gd}$, 2%Tm UCNPs. A strong and broad band at 1081 cm^{-1} , corresponding to the O-Si-O asymmetric stretching vibration, was observed in the spectrum (Supplementary Material: Fig. S5a). Also, a relatively weaker peak at 796 cm^{-1} attributed to the deformation vibration $\delta_{\text{Si-O}}$, appeared in the FT-IR spectrum of the silica coated UCNPs. These observations were indicative of successful fabrication of the

core-shell nanocrystals. The zeta potential value of the UCNPs without surface modification is around +20 (Supplementary Material: Fig. S5b). When the silica coating was conducted, the value decreased to about -20. It indicated that the SiO_2 was successfully coated on the surface of the UCNPs. As shown in Supplementary Material: Figure S5c,d, the EDX patterns showed that elements of Na, Yb, F, and Gd were all present in both hexagonal phase UCNPs and UCNP@ SiO_2 nanocrystals, whereas Si and O can only be found in the UCNP@ SiO_2 nanocrystals, which also provide evidence that the silica was successfully coated on the surface of the hexagonal phase UCNPs. Moreover, the presence of the amino group in the UCNP@ $\text{SiO}_2\text{-NH}_2$ nanocrystals was confirmed by the measurement of zeta potential (Supplementary Material: Fig. S6b). The zeta potential value of the UCNP@ $\text{SiO}_2\text{-NH}_2$ increased from -20 to around +60. Based on the UV-vis spectrum of UCNP-FA, it was confirmed that FA molecules were successfully conjugated on UCNP nanoparticles (Supplementary Material: Fig. S6).

Cytotoxicity of the core-shell nanocomposites

To evaluate the cytotoxicity of UCNP@ $\text{SiO}_2\text{-NH}_2$ and UCNP-FA nanocrystals, we conducted CCK assays on human gastric cancer cell line MGC-803 cells,

at 37 °C for 24h. The viability of untreated cells was assumed to be 100%. As shown in Figure 4(2), cell viabilities of MGC-803 cells incubated with different doses of UCNP@SiO₂-NH₂ for 24h were over 80%. As it shows in Figure 4(2), the cell viabilities of MGC-803 cells incubated with different concentration of UCNP-FA decreased comparing to UCNP@SiO₂-NH₂ treated cells, but most of the samples were over 80% viability, which fully suggests that prepared UCNPs and UCNP-FA have low cytotoxicity, and may be ideal candidates for further biological applications.

Fluorescent imaging of gastric cancer cells by confocal microscopy

The key for tumor targeted imaging based on nanoprobes is the ability of nanoprobes to target specific organelles or receptors. Folate receptor (FR) is a glycosylphosphatidylinositol (GPI)-anchored, high-affinity membrane folate binding protein overexpressed in a wide variety of human tumors, including >90% of gastric cancer [50, 51]. Meanwhile, distribution of folate receptor in normal tissues is highly restricted, which make folate receptor a useful target for cancer diagnosis and therapy [52-58].

To investigate the UCNP-FA nanoprobes' targeted ability, we studied the effects of folic acid conjugated UCNP@SiO₂-NH₂ nanoprobes on FR-positive MGC803 cells and FR-negative GES cells by using a modified Leica laser-scanning confocal microscopy (LSCM) with a CW laser at $\lambda=980$ nm as an additional excitation source [59]. Under CW excitation at $\lambda=980$ nm, we observed the luminescence signals in the MGC803 cells incubated with UCNP-FA nanoprobes for 1h at 37 °C (Fig. 5A), but no signal were detected in the MGC803 cells incubated with UCNP@SiO₂-NH₂ under the same condition (Fig. 5B). No luminescence signals were observed in the GES cells incubated with UCNP-FA nanoprobe (Fig. 5D). Competition experiments were conducted under the same conditions to confirm FA receptor's function. MGC803 cells with FA receptors were simultaneously incubated with UCNP-FA nanoprobes and excess FA for 3h at 37 °C, no luminescence signals were observed, as shown in Fig.5C. These results fully confirmed that UCNPs -FA could target and bind folate receptors overexpressed on gastric cancer cell line MGC-803 cells [60-65], and the fluorescent signal intensity in the gastric cancer cell line MGC803 cells is satisfactory.

Targeted imaging of in vivo gastric cancer cells by IVIS imaging system

To determine the feasibility of the use of FA conjugated silicon-modified NaYbF₄: 25%Gd, 2%Tm

UCNPs as a contrast reagent for targeted imaging of gastric cancer *in vivo*, we injected the prepared UCNP-FA nanoprobes into nude mice loaded with gastric cancer cells. Firstly, we transplanted human gastric cancer cell MGC803 cells into the subcutaneous position of nude mice, Secondly, when the tumor tissues grew up to 5mm in diameter, the nude mice were injected with UCNP-FA nanoprobes via tail vein. Then, the mice were imaged at 4h post injection by using a modified IVIS Lumina XR laser-scanning microscope, with a CW NIR laser at $\lambda=980$ nm as the excitation source. The emissions was collected nearby $\lambda=800$ nm. Figure 6 shows the *in vivo* whole-body images of mice injected with the UCNP-FA and UCNP@SiO₂-NH₂, the luminescent signals were collected through the skin of mice (without hair removal). Figure 6A showed that there was no autofluorescence interference phenomenon, and UCNP-FA nanoprobes could target gastric cancer tissues *in vivo*. We also investigated the distribution of UCNPs-FA nanoprobes in nude models, as shown in Supplementary Material: Figure S7, UCNPs-FA nanoprobes mainly distributed in the tumor tissues which further support UCNP-FA nanoprobes can target gastric cancers *in vivo*.

Conclusions

In summary, the α -phase NaYbF₄, 2%Tm and β -phase NaYbF₄: 25%Gd, 2%Tm nanocrystals with a uniform shape and size distribution as well as strong fluorescent signals were successfully synthesized through the OA/ IL two-phase synthesis system, and the amount of sodium oleate has an important effects on the transition of $\alpha \rightarrow \beta$ phase during the synthesis of β -phase UCNPs, especially increasing Na⁺ concentration could improve the fluorescent intensity of α -phase and β -phase UCNPs. The β -phase UCNPs were modified through silica coating, FA conjugated UCNP@SiO₂-NH₂ nanoprobes were successfully used for targeted NIR imaging of *in vivo* gastric cancer tissues, with high photostability and low autofluorescence interference. These results clearly show that the FA-conjugated NaYbF₄: 25%Gd, 2%Tm nanoprobes synthesized via the OA/IL two-phase system have great potential in applications such as NIR fluorescent imaging and targeted therapy of *in vivo* early gastric cancer in the near future.

Supplementary Material

Fig.S1 - Fig.S7.

<http://www.thno.org/v03p0210s1.pdf>

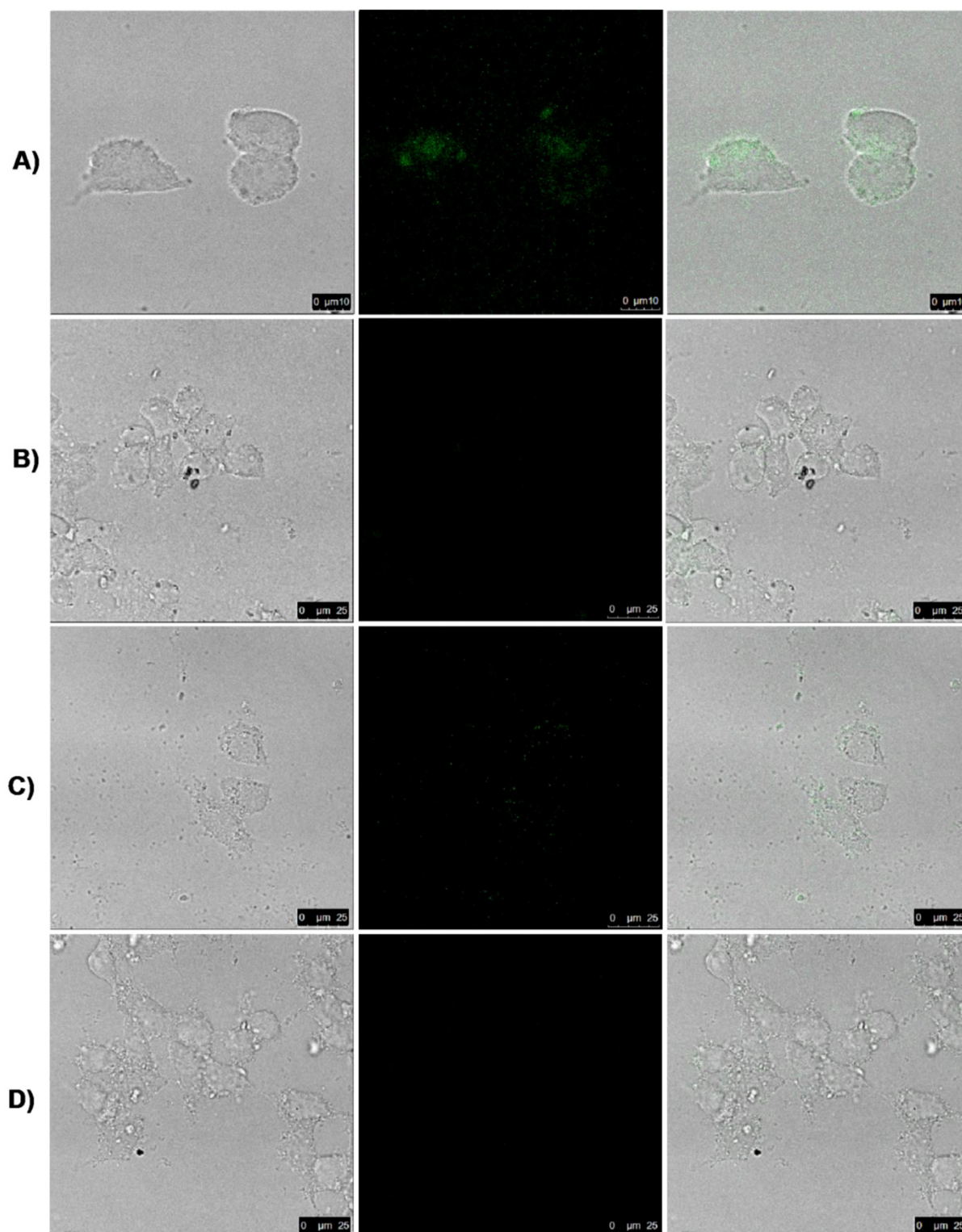


Figure 5. Laser scanning confocal microscopy (LSCM) images of MGC803 cells with FA receptor (A) and GES without FA receptor (D) cultivated with UCNP-FA nanocomposites (200 $\mu\text{g}/\text{mL}$) for 1 h at 37 $^{\circ}\text{C}$. Images (B) exhibit the cells incubated by the UCNP@SiO₂-NH₂ and images (C) show competition experiments in which MGC803 cells were incubated with excess free FA and UCNP-FA nanocomposites under the same conditions. All pictures were taken under the identical instrumental conditions.

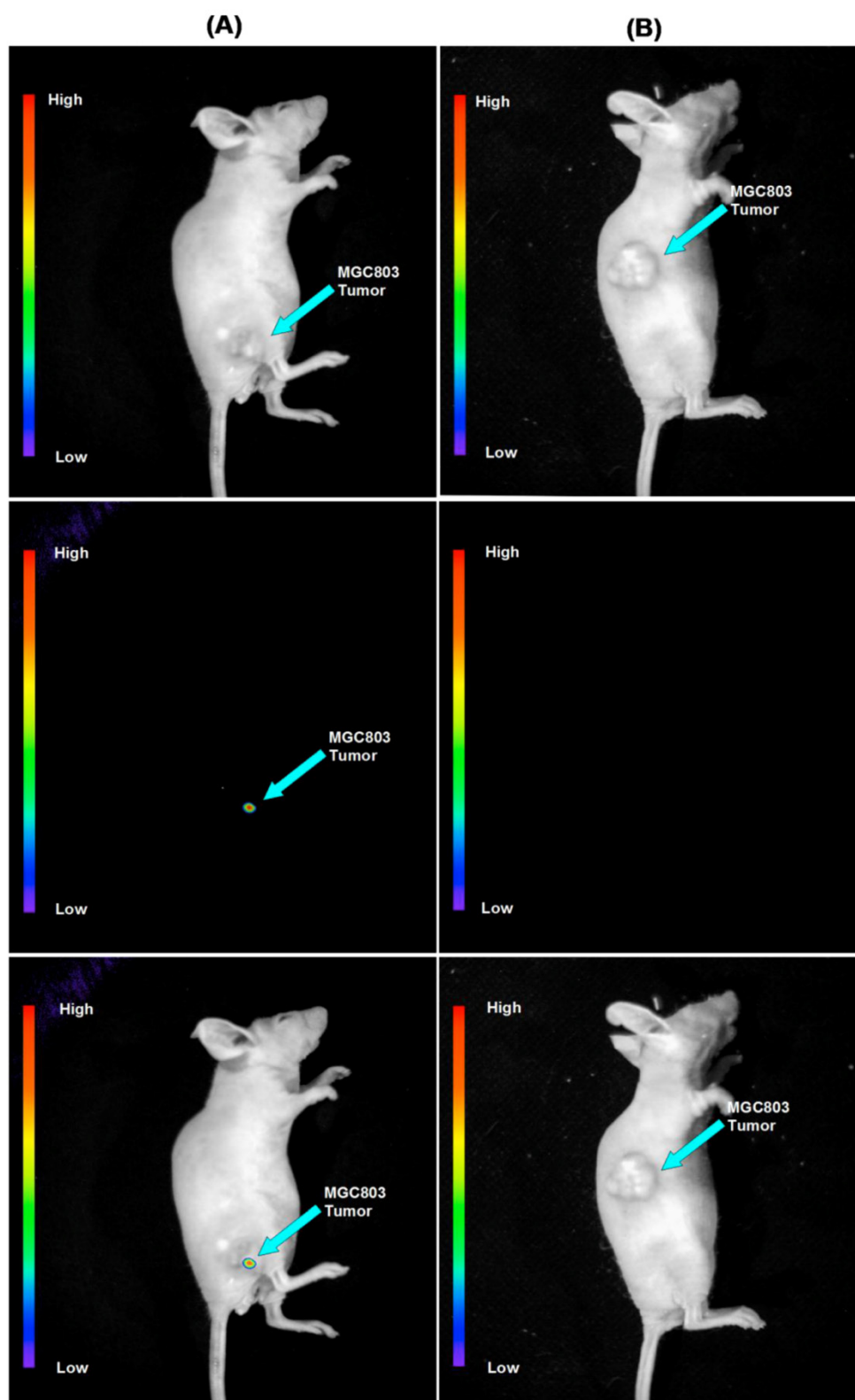


Figure 6. Targeted in vivo NIR luminescence imaging of subcutaneous MGC803 tumor (indicated by short arrows) after intravenous injection of NaYbF₄: 25%Gd, 2%Tm-FA (A) and NaYbF₄: 25%Gd, 2%Tm @SiO₂-NH₂. (B) nanoparticles for 4 h.

Acknowledgements

This work is supported by National Key Basic Research Program (973 Project) (No. 2010CB933901 and 2011CB933100), National 863 Hi-tech Project of China (No. F2007AA022004), Important National Science & Technology Specific Projects (2009ZX10004-311), National Natural Scientific Fund (No.81225010, 81101169 and 31100717), New Century Excellent Talent of Ministry of Education of China (NCET-08-0350), Specialized Research Fund for the Doctoral Program of Higher Education (No.20110073120072).

Competing Interests

The authors have declared that no competing interest exists.

References

- Wang F, Liu XG. Recent advances in the chemistry of lanthanide-doped upconversion nanocrystals. *Chem Soc Rev.* 2009; 38: 976-89.
- Wang F, Banerjee D, Liu YS, Chen XY, Liu XG. Upconversion nanoparticles in biological labeling, imaging, and therapy. *Analyst.* 2010; 135: 1839-54.
- Mao YB, Tran T, Guo X, Huang JY, Shih CK, Wang KL, et al. Luminescence of nanocrystalline erbium-doped yttria. *Adv Funct Mater.* 2009; 19: 748-54.
- Mao YB, Huang JY, Ostroumov R, Wang KL, Chang JP. Synthesis and luminescence properties of erbium-doped Y_2O_3 Nanotubes. *J Phys Chem C.* 2008; 112: 2278-85.
- Chandra S, Deepak FL, Gruber JB, Sardar DK. Synthesis, morphology, and optical characterization of nanocrystalline $Er^{3+}:Y_2O_3$. *J Phys Chem C.* 2010; 114: 874-80.
- Eliseeva SV, Bünzli JCG. Lanthanide luminescence for functional materials and bio-sciences. *Chem Soc Rev.* 2010; 39: 189-227.
- Carlos LDRA, Ferreira AS, Bermudez VDZ, Ribeiro SJL. Lanthanide-containing light-emitting organic-inorganic hybrids: a bet on the future. *Adv Mater.* 2009; 21: 509-34.
- Shalav A, Richards BS, Trupke T, Krämer KW, Güdel HU. Application of $NaYF_4:Er^{3+}$ up-converting phosphors for enhanced near-infrared silicon solar cell response. *Appl Phys Lett.* 2005;86:013505.
- Stouwdam JW, Veggel FJCM. Near-infrared emission of redispersible Er^{3+} , Nd^{3+} , and Ho^{3+} doped LaF_3 nanoparticles. *Nano Lett.* 2002; 2: 733-37.
- Bünzli JC. Lanthanide luminescence for biomedical analyses and imaging. *Chem Rev.* 2010; 110: 2729-55.
- Wang LY, Li YD. Controlled synthesis and luminescence of lanthanide doped $NaYF_4$ nanocrystals. *Chem Mater.* 2007; 19: 727-34.
- Shiohara A, Hoshino A, Hanaki K, Suzuki K, Yamamoto K. On the cyto-toxicity caused by quantum dots. *Microbiol Immunol.* 2004; 48: 669-75.
- Derfus AM, Chan WCW, Bhatia SN. Probing the cytotoxicity of semiconductor quantum dots. *Nano Lett.* 2004; 4: 11-18.
- Nirmal N, Dabbousi BO, Bawendi MG, Macklin JJ, Trautman JK, Harris TD, et al. Fluorescence intermittency in single cadmium selenide nanocrystals. *Nature.* 1996; 383: 802-04.
- Resch-Genger U, Grabolle M, Cavaliere JS, Nitschke R, Nann T. Quantum dots versus organic dyes as fluorescent labels. *Nat Methods.* 2008; 5: 763-75.
- Alivisatos AP. Semiconductor clusters, nanocrystals, and quantum dots. *Science.* 1996; 271: 933-37.
- Eggingel C, Widengren J, Rigler R, Seidel CAM. Photobleaching of fluorescent dyes under conditions used for single-molecule detection: evidence of two-step photolysis. *Anal Chem.* 1998; 70: 2651-59.
- Xiong LQ, Chen ZG, Yu MY, Li FY, Liu C, Huang HC. Synthesis, characterization, and in vivo targeted imaging of amine-functionalized rare-earth up-converting nanophosphors. *Biomaterials.* 2009; 30: 5592-00.
- Chatterjee DK, Rufaihah AJ, Zhang Y. Upconversion fluorescence imaging of cells and small animals using lanthanide doped nanocrystals. *Biomaterials.* 2008; 29: 937-43.
- Li ZQ, Zhang Y, Jiang S. Multicolor core/shell-structured upconversion fluorescent nanoparticles. *Adv Mater.* 2008; 20: 4765-79.
- Wang X, Li YD. A general strategy for nanocrystal synthesis. *Nature.* 2005; 437: 121-24.
- Wang F, Han Y, Lim CS, Lu YH, Wang J, Xu J, et al. Simultaneous phase and size control of upconversion nanocrystals through lanthanide doping. *Nature.* 2010; 463:1061-65.
- Wang LY, Li YD. Controlled synthesis and luminescence of lanthanide doped $NaYF_4$ nanocrystals. *Chem Mater.* 2007; 19: 727-34.
- Hu HY, Yang H, Huang P, Cui DX, Peng YQ, Zhang JC, et al. Unique role of ionic liquid in microwave-assisted synthesis of monodisperse magnetite nanoparticles. *Chem Commun.* 2010; 46: 3866-68.
- He M, Huang P, Zhang CL, Chen F, Wang C, Ma JB, et al. A general strategy for the synthesis of upconversion rare earth fluoride nanocrystals via a novel OA/ionic liquid two-phase system. *Chem Commun.* 2011; 47: 9510-12.
- He M, Huang P, Zhang CL, Hu HY, Bao CC, Guo G, et al. Dual phase-controlled synthesis of uniform lanthanide-doped $NaGdF_4$ upconversion nanocrystals via an OA/ionic liquid two-phase system for in vivo dual-modality Imaging. *Adv Funct Mater.* 2011; 21: 4470-77.
- He M, Huang P, Zhang CL, Ma JB, He R, Cui DX. Phase-and-size controllable synthesis of hexagonal upconversion rare-earth fluoride nanocrystals via an oleic acid/ ionic liquid two-phase system. *Chem Eur J.* 2012; 18: 5954-69.
- Chen GY, Ohulchanskyy TY, Kumar T, Ågren H, Prasad PN. Ultrasmall monodisperse $NaYF_4:Yb^{3+}/Tm^{3+}$ nanocrystals with enhanced near-infrared to near-infrared upconversion photoluminescence. *ACS Nano.* 2010; 4: 3163-68.
- Reubinoff BE, Pera MF, Fong CY, et al. Embryonic stem cell lines from human blastocysts: somatic differentiation in vitro. *Nat Biotechnol.* 2000; 18: 399-04.
- Schottenfeld D, Fraumeni JF. *Cancer Epidemiology and Prevention.* USA: Oxford University Press. 2006.
- Power D, Kelsen D, Shah M. Advanced gastric cancer-slow but steady progress. *Cancer Treat Rev.* 2010; 36: 384-92.
- Hartgrink H, Jansen E, van Grieken N, van de Velde C. Gastric cancer. *Lancet.* 2009; 374: 477-90.
- Crew K, Neugut A. Epidemiology of gastric cancer. *World J Gastroenterol.* 2006; 12: 354-62.
- Cui D, Zhang L, Yan X, Zhang L, Xu J, Guo Y, et al. A microarray-based gastric carcinoma prewarning system. *World J Gastroenterol.* 2005; 11: 1273-82.
- Zhang X, Li D, Wang C, Zhi X, Zhang C, Wang K, et al. A CCD-based reader combined quantum dots-labeled lateral flow strips for ultrasensitive quantitative detection of anti-HBs antibody. *J Biomed Nanotechnol.* 2012; 8: 372-79.
- Wang K, Ruan J, Qian Q, Song H, Bao C, Zhang X, et al. BRCA1 monoclonal antibody conjugated fluorescent magnetic nanoparticles for in vivo targeted magnetofluorescent imaging of gastric cancer. *Journal of Nanobiotechnology.* 2011; 9: 23.
- Huang P, Li Z, Lin J, Yang D, Gao G, Xu C, et al. Photosensitizer-conjugated magnetic nanoparticles for in vivo simultaneous magnetofluorescent imaging and targeting therapy. *Biomaterials* 2011; 32: 3447-58.
- Kong Y, Chen J, Gao F, Li W, Xu X, Omar P, et al. A multifunctional ribonuclease-A-conjugated CdTe quantum dot cluster nanosystem for synchronous cancer imaging and therapy. *Small.* 2010; 6: 2367-73.
- Huang P, Xu C, Lin J, Wang C, Wang X, Zhang C, et al. Folic acid-conjugated graphene oxide loaded with photosensitizers for targeting photodynamic therapy. *Theranostics.* 2011;1: 240-50.
- Li Z, Huang P, Zhang X, Lin J, Yang S, Liu B, et al. RGDconjugated dendrimer-modified gold nanorods for in vivo tumor targeting and photothermal therapy. *Mol Pharm.* 2009; 7: 94-04.
- Singh R, Nalwa H. Medical applications of nanoparticles in biological imaging, cell labeling, antimicrobial agents, and anticancer nanodrugs. *J Biomed Nanotechnol.* 2011; 7: 489-03.
- Lee H, Nguyen Y, Muthiah M, Vu-Quang H, Namgung R, Kim W, et al. MR traceable delivery of p53 tumor suppressor gene by PEI-functionalized superparamagnetic iron oxide nanoparticles. *J Biomed Nanotechnol.* 2012; 8: 361-71.
- Xu G, Yong K, Roy I, Kopwithaya A. FGF2-labeled semiconductor nanocrystals as luminescent biolabels for imaging neuroblastoma cells. *J Biomed Nanotechnol.* 2010; 6: 641-47.

44. Ding J, Zhao J, Cheng K, Liu G, Xiu D. In vivo photodynamic therapy and magnetic resonance imaging of cancer by TSPP-coated Fe₃O₄ nanoconjugates. *J Biomed Nanotechnol.* 2010; 6: 683-86.
45. Wei F, Lu FQ, Zhang XR, Chen DP. Synthesis of oil-dispersible hexagonal-phase and hexagonal-shaped NaYF₄:Yb,Er nanoplates. *Chem Mater.* 2006; 18: 5733-37.
46. Park J, An KJ, Hwang YS, Park JG, Noh HJ, Kim JY, et al. Ultra-large-scale syntheses of monodisperse nanocrystals. *Nat Mater.* 2004; 3: 891-95.
47. Wang X, Zhuang J, Peng Q, Li YD. Hydrothermal synthesis of rare-earth fluoride nanocrystals. *Inorg Chem.* 2006; 45: 6661-65.
48. Mai HX, Zhang YW, Si R, Yan ZG, Sun LD, You LP, et al. High-quality sodium rare-earth fluoride nanocrystals: controlled synthesis and optical properties. *J Am Chem Soc.* 2006; 128: 6426-36.
49. Hu H, Yu MX, Li FY, Chen ZG, Gao X, Xiong LQ, et al. Facile epoxidation strategy for producing amphiphilic up-converting rare-earth nanophosphors as biological labels. *Chem Mater.* 2008; 20: 7003e9.
50. Kulakovich O, Strekal N, Yaroshevich N, Maskevich S, Gaponenko S, Nabiev I, et al. Enhanced luminescence of CdSe quantum dots on gold colloids. *Nano Lett.* 2002; 2: 1449-52.
51. Garin-Chesa P, Campbell I, Saigo PE, Lewis JLJ, Old LJ, Rettig WJ. Trophoblast and ovarian cancer antigen LK26. Sensitivity and specificity in immunopathology and molecular identification as a folate-binding protein. *Am J Pathol.* 1993; 42: 557-67.
52. Ross JF, Chaudhuri PK, Ratnam M. Differential regulation of folate receptor isoforms in normal and malignant tissues in vivo and in established cell lines. *Cancer.* 1994; 73: 2432-43.
53. Leamon CP, Low PS. Folate-mediated targeting: from diagnostics to drug and gene delivery. *Drug Discovery Today.* 2001; 6: 44-51.
54. Leamon CP, Low PS. Selective targeting of malignant cells with cytotoxin-folate conjugates. *Drug Targeting.* 1994; 2: 101-112.
55. Qu LH, Peng ZA, Peng XG. Alternative routes toward high quality CdSe nanocrystals. *Nano Lett.* 2001; 1: 333-37.
56. Lu YJ, Low PS. Folate targeting of haptens to cancer cell surfaces mediates immunotherapy of syngeneic murine tumors. *Cancer Immunol Immunother.* 2002; 51: 153-62.
57. Lu N, Chen XD, Molenda D, Naber A, Fuchs H, Talapin DV, et al. Lateral patterning of luminescent CdSe nanocrystals by selective dewetting from self-assembled organic templates. *Nano Lett.* 2004; 4: 885-88.
58. Ward CM. Folate-targeted non-viral DNA vectors for cancer gene therapy. *Curr Opin Mol Ther.* 2000; 2: 182-87.
59. Yu MX, Li FY, Chen ZG, Hu H, Zhan C, Huang CH. Laser scanning up-conversion luminescence microscopy for imaging cells labeled with rare-earth nanophosphors. *Anal Chem.* 2009; 81: 930-35.
60. Chen X. Integrin Targeted imaging and therapy. *Theranostics.* 2011; 1: 28-29.
61. Niu G, Chen X. Molecular imaging with activatable reporter systems. *Theranostics.* 2012; 2: 413-23.
62. Zhang F, Zhu L, Liu G, et al. Multimodality imaging of tumor response to Doxil. *Theranostics* 2011; 1: 302-309.
63. Oghabian MA, Farahbakhsh NM. Potential use of nanoparticle based contrast agents in MRI: a molecular imaging perspective. *J Biomed Nanotechnol.* 2010; 6: 203-13.
64. Lai P, Nathoo S, Ku T, et al. Real-time imaging of interactions between dipalmitoylphosphatidylcholine monolayers and gelatin based nanoparticles using brewster angle microscopy. *J Biomed Nanotechnol.* 2010; 6: 145-52.
65. Navarro FP, Berger M, Guillermet S, et al. Lipid nanoparticle vectorization of indocyanine green improves fluorescence imaging for tumor diagnosis and lymph node resection. *J. Biomed. Nanotechnol.* 2012; 8: 730-41.